Article

A Stress-Strain Model for Unconfined in Compression considering the Size Effect

Keun-Hyeok Yang [1], Yongjei Lee [1] and Ju-Hyun Mun [1,*]

[1] Department of Architectural Engineering, Kyonggi University, Suwon 16227, Republic of Korea; yangkh@kgu.ac.kr (KH. Y.); yongjei@gmail.com (Y.L.)
* Correspondence: mjh@kgu.ac.kr; Tel.: +82-(0)31-249-1477

Abstract: In this study, the model proposed by Yang et al. to generalize the stress–strain model for unconfined concrete with consideration of the size effect is expanded. Sim et al.'s compressive strength model that is based on the function of specimen width and aspect ratio was used for the maximum stress. In addition, a strain at the maximum stress was formulated as a function of compressive strength by considering the size effect using the regression analysis of datasets compiled from a wide variety of specimens. The descending branch after the peak stress was formulated with consideration of less dissipated area of fracture energy with the increase in specimen width and aspect ratio in the compression damage zone (CDZ) model. The key parameter for the slope of the descending branch was formulated as a function of specimen width and aspect ratio, concrete density, and compressive strength of concrete considering the size effect. Consequently, a rational stress–strain model for unconfined concrete was proposed. This model explains the trends of the peak stress and strain at the peak stress to decrease and the slope of the descending branch to increase, as the specimen width and aspect ratio increase. The proposed model agrees well with the test results, irrespective of the compressive strength of concrete, concrete type, specimen width and aspect ratio. In particular, the proposed model for the stress–strain curve rationally considered the effect of decreasing peak stress and increasing the descending branch slope, with the increase in specimen width and aspect ratio.

Keywords: stress-strain model; size effect; fracture energy; softening

1. Introduction

The stress–strain relationship for unconfined concrete is a fundamental material property for the design and analysis of structural elements [1–3]. Generally, stress–strain relationship is affected by the type and compressive strength of concrete, as well as the maximum diameter of aggregate, specimen width, and aspect ratio in the descending branch from the crack propagation in fracture zone [4–7]. To study this trend, researchers [5, 8–10] proposed concrete compressive strength models with the size effect in various approaches based on the fracture energy theory. Bažant and Planas [8] reported that concrete compressive strength was considerably affected by the specimen width, indicating that it decreased by 10%, as the specimen width increased by twice. Sim et al. [5] emphasized that the decreasing rate of concrete compressive strength with the increase in the specimen width in a normal weight concrete (NWC) was more notable than that in lightweight concrete (LWC). In particular, because cracks at the failure zone for LWC pass through lightweight aggregate particles, the crack band zone is more localized in LWC than NWC. Hence, the size effect of concrete on the peak stress and descending branch behavior that is directly related to crack propagations in the failure zone could be more notable in LWC than NWC [5]. However, for the size effect of concrete on the descending branch from the crack propagation in a localized crack band zone, only few studies have been conducted. In particular, very little literature on the size effect in LWC is available. Furthermore, the existing proposed models [6, 7] for the stress–strain relationship

regarding the size effect of concrete on the descending branch, are typically determined from NWC test datasets, rather than from LWC, with limited ranges of variables.

Markeset and Hillerborg [6] generalized the compression damage zone (CDZ) model to consider the size effect of concrete on the descending branch using a function of strain dissipated by the shear band including the fracture energy. However, the primary factors to the descending branch behavior in Markeset and Hillerborg's model are drawn from the limited ranges of variables. In addition, this model is limited for a practical equation because the information about the strain of the starting point for the softening behaviour is not available. Samani and Attard [7] considered the size effect of concrete by applying the CDZ model [6] to the descending branch in Attard and Setunge's model [11]. As the Samani and Attard [7]'s model has an identical strain model of shear band as Markeset and Hillerborg's [6], information regarding the material property factors is necessary to predict the stress–strain relationship. In addition, the descending branch of these models does not fully consider the effect of aggregate property on crack propagation and the localized fracture zone. For example, in LWC, the contribution of stress transfer at the crack plane for aggregate interlocking action is little [5] because most of the cracks at the failure plane pass through lightweight aggregate particles. In addition, the strength and elastic modulus of aggregate such as magnetite in heavyweight concrete (HWC) are typically higher than those of NWC, which can cause a wider fracture zone by crack propagation. Hence, the size effect of LWC and HWC could be different from that of NWC because the size effect on concrete depends on areas of failure and crack propagation in the fracture zone. However, as the existing models [6, 7] incorporating the size effect of concrete on the descending branch were derived from limited NWC test datasets, limited number of studies for the size effect of concrete using light and heavyweight aggregates are available.

The objective of this study is to propose a model for the stress–strain curve considering the size effect of various concrete types. In this model, the basic formula for the stress–strain curve and the key parameter that determines the slopes of the ascending and descending branches established by Yang et al. [1] was used to generate a complete nonlinear curve. The concrete compressive strength model proposed by Sim et al. [5] that considers the size effect was used for the peak stress. The strain at the peak stress was generalized with a simple equation using the regression analysis of datasets compiled from specimens with various ranges of specimen width, aspect ratio, concrete compressive strength, and density. In the softening behavior of the descending branch in the stress–strain relationship, the size effect and fracture energy were considered using Markeset and Hillerborg's CDZ model [6]. The key parameter for the softening behavior was determined from the secant modulus joining the origin and 0.5 $f_{SE}^{'}$, where $f_{SE}^{'}$ is the compressive strength of concrete considering the size effect. The strain model at 0.5 $f_{SE}^{'}$ to determine the key parameter was generalized with various ranges of variables using regression analysis. Finally, the key parameter that determines the slope of the descending branch was formulated as a function of specimen width and aspect ratio, concrete density, and concrete compressive strength, considering the size effect using parametric numerical analysis. The accuracy of the proposed model was evaluated using a normalized root–mean–square error obtained from the comparisons of predicted curves with the test results.

2. Database

To formulate the material properties, Yang et al. [1] compiled 3295 datasets for the elastic modulus of concrete (E_c), 415 datasets for strain at the peak stress (ε_0), and 96 datasets for strain at 50% of the peak stress ($\varepsilon_{0.5}$) in the descending branch. In the compiled datasets, the concrete compressive strength ($f_c^{'}$) and density (ρ_c) varied from 8.4 MPa to 170 MPa and from 1200 kg/m^3 to 4500 kg/m^3, respectively. To apply the effect of concrete type to the empirical formulation, the datasets were divided into LWC, NWC, and HWC according to ρ_c. The concrete density (ρ_c) varied from 1200 kg/m^3 to 2000 kg/m^3 for LWC, from 2000 kg/m^3 to 2500 kg/m^3 for NWC, and from 2500 kg/m^3 to 4500 kg/m^3 for HWC. The datasets compiled by Yang et al. [1] were all measured from

Preprints (www.preprints.org) | NOT PEER-REVIEWED | Posted: 22 August 2018 doi:10.20944/preprints201808.0392.v1

a cylinder of diameter 100 mm and height 200 mm. Hence, the datasets compiled by Yang et al. [1] lack the test results for the size effect of concrete. To compensate for this, additional test results for the size effect of concrete were compiled. The compiled additional test results [4, 5, 23–25] for the stress–strain relationship were 38 datasets for LWC, and 20 datasets for NWC, as shown in Table 1. In the datasets, specimen width (d), aspect ratio (h/d), $f_c^{'}$, and ρ_c were varied from 50 mm to 350 mm, 0.5 to 5.5, 4 mm to 20 mm, 17.1 MPa to 90.2 MPa, and 1500 kg/m^3 to 2464 kg/m^3, respectively. The specimen width (d) and h/d were varied from 100 mm to 350 mm and 1 to 2 for LWC, and 50 mm to 100 mm and 0.5 to 5.5 for NWC, respectively. Meanwhile, the datasets still lack the test results for the size effect on HWC, because the relevant test results are not available in the literature. It is noteworthy that the reliability of the proposed model for the stress–strain relationship of HWC was evaluated based only on datasets compiled by Yang et al. [1].

Table 1. Distribution of parameters in the dataset for stress–strain curves.

	Range	**–20**	**20–40**	**40–60**	**60–80**	**80–100**	**Total**
$f_c^{'}$	LWC	4	26	8	0	0	38
	NWC	2	3	10	0	5	20
	Range	**–50**	**50–100**	**100–200**	**200–300**	**300–400**	**Total**
d	LWC	0	34	1	2	1	38
	NWC	3	17	0	0	0	20
	Range	**0.5–1**	**1–2**	**2–3**	**3–4**	**4–6**	**Total**
h/d	LWC	3	35	0	0	0	38
	NWC	4	5	3	4	4	20
	Range	**4**	**4–10**	**10–15**	**15–20**	**20–**	**Total**
d_a	LWC	1	2	2	33	0	38
	NWC	0	14	0	6	0	20

3. Model Generalization

3.1. Basic approach

The stress–strain relationship for unconfined concrete in compression is a parabola with an ascending and descending branch, and a vertex at the peak stress [1–3]. This shape can be generalized using the following equation [1].

$$y = \frac{(\beta_1 + 1)x}{x^{\beta_1 + 1} + \beta_1} \tag{1}$$

where $y = f_c / f_c^{'}$ is the normalized stress, $x = \varepsilon_c / \varepsilon_0$ is the normalized strain, f_c and ε_c are the concrete stress and strain at some point in stress–strain curve, respectively, and β_1 is the key parameter that determines the slopes of the ascending and descending branches. The ascending branch can be determined from E_c, which is defined as the slope of the line joining the origin and 40% of the peak stress. In addition, the descending branch can be determined from the secant modulus joining the origin and 0.5 $f_c^{'}$ [1]. In accordance with Yang et al.'s model [1], the equation for the key parameter β_1 that determines the slopes of the ascending and descending branches can be expressed as follows.

$$0.4(X_a)^{\beta_1 + 1} + (0.4 - X_a)\beta_1 - X_a = 0 \qquad \text{for} \quad \varepsilon_c \le \varepsilon_0 \tag{2}$$

$$(X_d)^{\beta_1 + 1} + (1 - 2X_d)\beta_1 - 2X_d = 0 \qquad \text{for} \quad \varepsilon_c > \varepsilon_0 \tag{3}$$

where $X_a = 0.4 f_c^{'} / E_c \varepsilon_0$ and $X_d = \varepsilon_{0.5} / \varepsilon_0$.

Preprints (www.preprints.org) | NOT PEER-REVIEWED | Posted: 22 August 2018 doi:10.20944/preprints201808.0392.v1

Bažant [9] proposed the crack band zone by a crack width with micro cracks propagation for concrete failure. In addition, Bažant [9] idealized the crack band width as a function of d_a, assuming that micro cracks propagated the interfaces between aggregates and pastes. Sim et al. [5] proposed a smaller area of crack band zone in LWC than NWC as shown in Fig. 1, based on the crack band theory [9]. This model includes the effect of reduced area of the crack band zone caused by the cracks at the failure zone passing through lightweight aggregate particles, and also considers the size effect on concrete due to the decrease in α/d as d increases, where α is the crack length. Sim et al. [5] derived the equation for the compressive strength of concrete (f'_{SE}) considering the size effect from the energy balance, in that the strain energy for concrete deformation dissipated by the crack band zone equals the total energy consumed by the band of the axial splitting micro cracks. The proposed model is as follows.

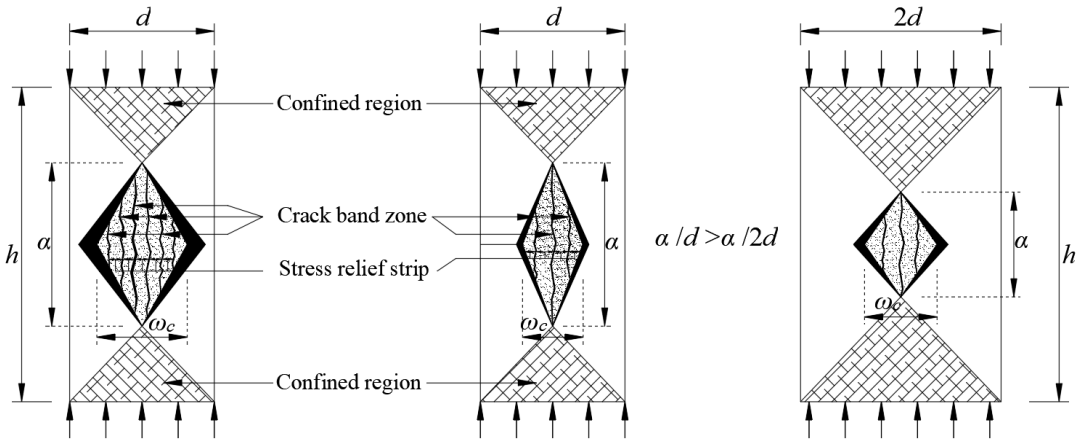

Figure 1. Idealized crack band zone at peak stress based on concrete fracture mechanics

$$f'_{SE} = \left[\frac{A_1 \sqrt{\frac{1}{k}\left(\frac{h}{d}\right)^{X_4}}}{\left[1 + B_1 \frac{d}{d_a^{X_1}} \left(\frac{\rho_c}{2300}\right)^{-X_2}\right]^{0.5}} \right] f'_c \tag{4}$$

where A_1 is $\sqrt{\frac{nk_1X_3}{F_2}\left(1-\frac{E_c}{E_t}\right)}$, n is number of micro cracks in the band, B_1 is $\frac{F_1}{F_2}$, F_1 is $\frac{\partial F}{\partial \alpha_1}$, F_2 is $\frac{\partial F}{\partial \alpha_2}$, F is $f(\alpha_1,\alpha_2)$, α_1 and α_2 are the modification factors to account for the volume of the crack band zone, E_t is the strain–softening modulus, and X_1, X_2, X_3, and X_4 are experimental constants. In Eq. (4), f'_c indicates the compressive strength of concrete measured in a reference specimen with d of 150 mm and h/d of 2. From Eq. (4), this indicates that f'_c is considerably affected by the functions of d, h/d and ρ_c [5, 8–10]. Sim et al. [5] determined the functions of A_1, B_1, $d_a^{X_1}$, k, X_2, and X_4 in Eq. (4) from 1509 datasets with LWC and NWC test results, and proposed as follows.

$$f'_{SE} = \left[\frac{0.9\sqrt{\left(\frac{h}{d}\right)^{-0.6}}}{\left[1 + 0.017d\left(\frac{\rho_c}{2300}\right)^{-1}\right]^{0.5}} + 0.63 \right] f'_c \tag{5}$$

In the model of Sim et al. [5], Eq. (5) considers a function of ρ_c that reflects the trend that the size effect is more notable in LWC than NWC. The stress–strain relationship is shown in Fig. 2, using

Preprints (www.preprints.org) | NOT PEER-REVIEWED | Posted: 22 August 2018 doi:10.20944/preprints201808.0392.v1

Eq. (5) for the peak stress. In Fig. 2, the key parameter β_1 can be determined with the following equations.

$$0.4(X_{a1})^{\beta_1+1}+(0.4-X_{a1})\beta_1-X_a=0 \qquad \text{for } \varepsilon_c \le \varepsilon_{SE} \tag{6}$$

$$(X_{d1})^{\beta_1+1}+(1-2X_{d1})\beta_1-2X_{d1}=0 \qquad \text{for } \varepsilon_c > \varepsilon_{SE} \tag{7}$$

where $X_{a1}=0.4f_{SE}^{'}/E_c\varepsilon_{SE}$, $X_{d1}=\varepsilon_{SE0.5}/\varepsilon_{SE}$, ε_{SE} is the strain at the peak stress considering the size effect, and $\varepsilon_{SE0.5}$ is the strain at $0.5f_{SE}^{'}$ after the peak stress. In Eq. (1), the key parameter β_1 that determines the ascending and descending branches requires information about the functions of E_c, ε_{SE}, and $\varepsilon_{SE0.5}$, as expressed in Eq. (6) and (7).

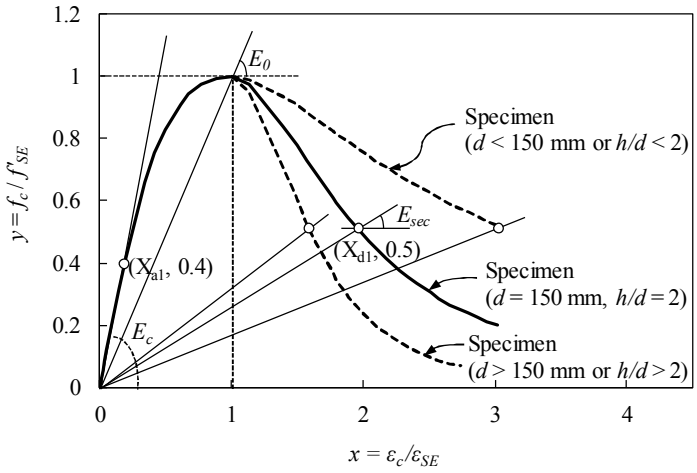

Figure 2. Generalization of compressive stress–strain curve of concrete considering the size effect

3.2 Determination of β_1 in ascending branch

The size effect on concrete is based on the crack band theory indicating the crack width with the propagation of micro cracks, as shown in Fig. 3. It implies that the behavior of the points of 'O' and 'A' without any cracks in the graph is not affected by the size effect. In addition, Taylor and Broms [26] assumed that the first point of decreasing stiffness in the stress–strain relationship is identical to an occurrence point of bond crack and reported that this point was between 30% to 42% of $f_c^{'}$ from the test results. Considering E_c is typically defined at $0.4f_c^{'}$ [27], the size effect of concrete is slight because no micro crack is likely to occur within $0.4f_c^{'}$. Consequently, Yang et al.'s model [1], a function of $f_c^{'}$ and ρ_c as follows, was used for E_c.

$$E_c=8470\left(f_c^{'}\right)^{1/3}(\rho_c/2300)^{1.17} \tag{8}$$

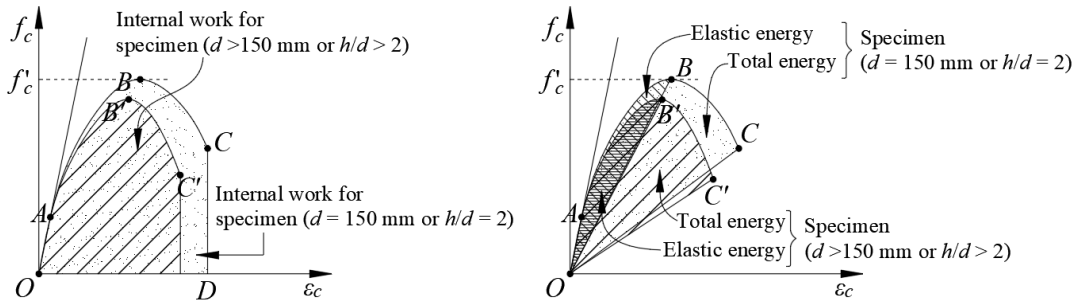

Figure 3. Fracture energy for concrete failure.

Preprints (www.preprints.org) | NOT PEER-REVIEWED | Posted: 22 August 2018 doi:10.20944/preprints201808.0392.v1

Meanwhile, as shown in Fig. 2, Eq. (5) can be expressed as follows from the relation of $f_{SE}^{'}$ and E_0.

$$\varepsilon_{SE} = \left[\frac{0.9\sqrt{\left(\frac{h}{d}\right)^{-0.6}}}{\left[1+0.017d\left(\frac{\rho_c}{2300}\right)^{-1}\right]^{0.5}} + 0.63 \right] \frac{f_c^{'}}{E_0} \tag{9}$$

Consequently, ε_{SE} can be expressed as follows.

$$\varepsilon_{SE} = f_{SE}^{'} / E_0 \tag{10}$$

where E_0 is the secant modulus joining the origin and the peak stress. Eq. (10) shows that ε_{SE} is fully affected by the functions of $f_{SE}^{'}$ and E_0. However, a dataset or predicted model for E_0 is not available. Hence, E_0 can be expressed as follows using a certain relation with E_c, as shown in Fig. 2.

$$\varepsilon_{SE} = \chi\left(f_{SE}^{'} / E_c\right) \tag{11}$$

where χ is a coefficient to account for the relation of E_0 and E_c, which can be determined from the test results. From the datasets compiled in this study, Eq. (11) can be expressed as follows (Fig. 4).

$$\varepsilon_{SE} = 0.0016\exp\left[220\left(f_{SE}^{'} / E_c\right)\right] \tag{12}$$

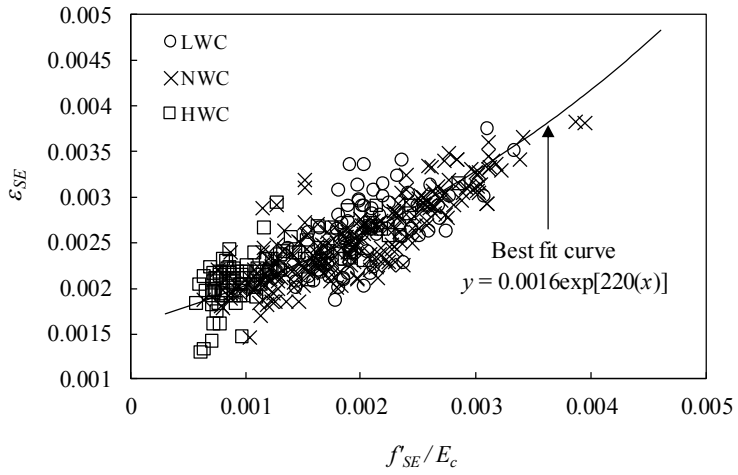

Figure 4. Nonlinear regression analysis for ε_{SE}.

The key parameter β_1 that determines the slope of the ascending branch can be solved by substituting Eq. (8) and Eq. (12) into Eq. (6). The key parameter β_1 was calculated using the Newton–Raphson method, identical to Yang et al.'s model [1]. Finally, the key parameter β_1 was formulated using the analytical parametric study. Because E_c is not affected by the size effect while ε_{SE} is affected by it, the ranges of variables $f_c^{'}$, ρ_c, d, and h/d were selected to be from 10 MPa to 180 MPa, 1400 kg/m^3 to 4000 kg/m^3, 50 mm to 500 mm and 0.5 to 5, respectively, from the parametric study. From the analytical results, a statistical optimization was performed to generalize the key parameter β_1 that determines the slope of the ascending branch as follows (Fig. 5).

$$\beta_1 = 0.33\exp\left[0.42\left(f_{SE}^{'}/10\right)\left(2300/\rho_c\right)^{1.5}\right] \quad \text{for} \quad \varepsilon_c \le \varepsilon_{SE} \tag{13}$$

Preprints (www.preprints.org) | NOT PEER-REVIEWED | Posted: 22 August 2018 doi:10.20944/preprints201808.0392.v1

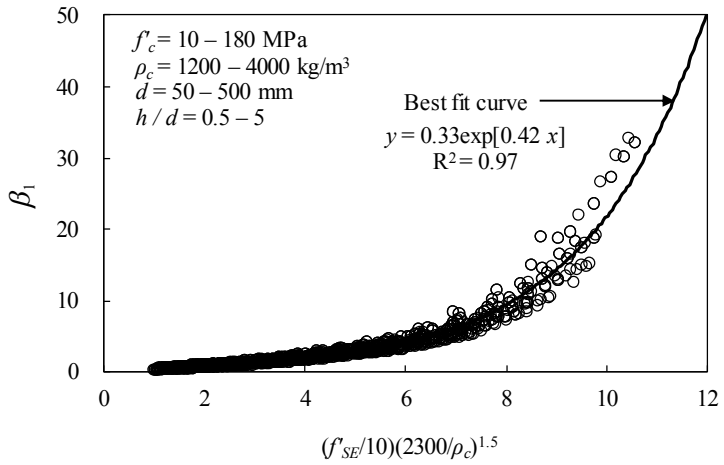

Figure 5. Formulation of key parameter β_1 in ascending branch

Eq. (13) shows that the slope of the ascending branch increases with the increase in f'_{SE} or decrease in ρ_c. Consequently, the slope of the ascending branch includes the size effect of concrete with the generalization of a function of f'_{SE}, considering the parameters d and h/d.

3.3 Determination of β_1 in descending branch

The descending branch behavior after the peak stress is determined from the localized deformation developed in the damaged or failure zone, while the undamaged zone elastically unloads [6]. Hence, the undamaged zone is generated only when h is greater than the damaged zone height (h_d). From this finding, Markeset and Hillerborg [6] idealized the CDZ model generated from the longitudinal tensile splitting cracks and diagonal tensile band crack in the damaged zone (Fig. 6). According to Markeset and Hillerborg [6], the total strain ε_c in the softening behavior is the sum of the strain during the unloading region after the peak stress in the undamaged zone, the strain while tensile splitting crack occurs in the longitudinal direction, and the strain caused by the diagonal shear band (ω/h).

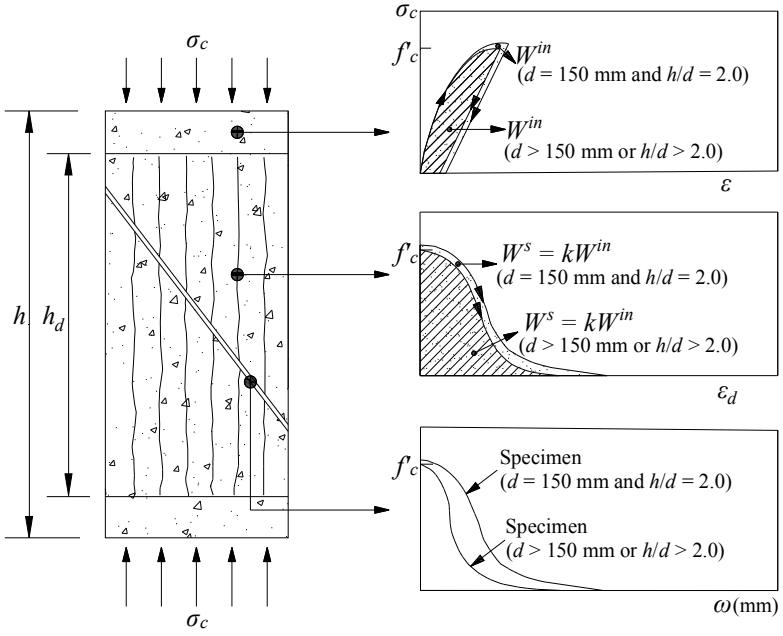

Figure 6. Compression damage zone (CDZ) model [6]

Preprints (www.preprints.org) | NOT PEER-REVIEWED | Posted: 22 August 2018 doi:10.20944/preprints201808.0392.v1

$$\varepsilon_c = \varepsilon + \varepsilon_d (h_d / h) + \omega / h \quad \text{for} \quad h > h_d \tag{14.a}$$

$$\varepsilon_c = \varepsilon + \varepsilon_d + \omega / h \quad \text{for} \quad h \le h_d \tag{14.b}$$

where h_d is the height of the region propagated by the longitudinal tensile splitting cracks. ω is the localized deformation assumed as between 0.4 and 0.7 for NWC, and less than 0.3 for LWC. Assuming that the strain (ε_d) in the region propagated by the longitudinal tensile splitting cracks is proportional to the fracture energy (G_F), it can be proposed as follows.

$$\varepsilon_d = \left[\frac{2kG_F}{\gamma(1+k)f_c^{'}}\right]\left(\frac{f_c^{'} - f_c}{f_c^{'}}\right)^{0.8} \tag{15}$$

where k is the factor based on the material properties that can be assumed as 3 for NWC, and 1 for LWC. γ is the factor with specimen height that can be assumed as 1.25 mm for d_a of 16 mm. As expressed in Eq. (15), the CDZ model proposed by Markeset and Hillerborg [6] includes a function of G_F, in the descending branch. However, both k and ω, require calibration according to various concrete types because they are based on the material properties, which is too demanding for a practical application. Furthermore, because γ is proposed only for a d_a of 16 mm, the use of a practical equation is limited for other specimens with larger aggregate. Hence, to obtain information about these factors, a comprehensive test is required with various influencing parameters including concrete type, d, h/d, and d_a. To improve Markeset and Hillerborg's model [6], the key parameter β_1 by Yang et al. [1] was applied to the descending branch behavior. The peak stress from Eq. (5) by Sim et al. [5] and $\varepsilon_{SE0.5}$ from Eq. (14) are used to produce the following equation.

$$\varepsilon_{SE0.5} = \left(\varepsilon_{SE} - \frac{f_{SE}^{'}}{E_c}\right) + \left(\frac{2kG_F}{\gamma(1+k)f_{SE}^{'}}\right)\left(\frac{f_{SE}^{'} - 0.5f_{SE}^{'}}{f_{SE}^{'}}\right)^{0.8}\frac{h_d}{h} + \frac{\omega}{h} \quad \text{for} \quad h > h_d \tag{16.a}$$

$$\varepsilon_{SE0.5} = \left(\varepsilon_{SE} - \frac{f_{SE}^{'}}{E_c}\right) + \left(\frac{2kG_F}{\gamma(1+k)f_{SE}^{'}}\right)\left(\frac{f_{SE}^{'} - 0.5f_{SE}^{'}}{f_{SE}^{'}}\right)^{0.8} + \frac{\omega}{h} \quad \text{for} \quad h \le h_d \tag{16.b}$$

where ε_{SE}, E_c and $f_{SE}^{'}$ are known values. In eq. (16), the first term in the right is moved to the left side and can be arranged as follows.

$$\varepsilon_{SE0.5} - \left(\varepsilon_{SE} - \frac{f_{SE}^{'}}{E_c}\right) = \left(\frac{2kG_F}{\gamma(1+k)f_{SE}^{'}}\right)\left(0.5^{0.8}\right)\frac{h_d}{h} + \frac{\omega}{h} \quad \text{for} \quad h > h_d \tag{17.a}$$

$$\varepsilon_{SE0.5} - \left(\varepsilon_{SE} - \frac{f_{SE}^{'}}{E_c}\right) = \left(\frac{2kG_F}{\gamma(1+k)f_{SE}^{'}}\right)\left(0.5^{0.8}\right) + \frac{\omega}{h} \quad \text{for} \quad h \le h_d \tag{17.b}$$

The factors of k and ω could be intimately related to ρ_c because they are based on the aggregate property. In addition, γ is related to the specimen height and proportional to the average space of the longitudinal tensile splitting cracks. These indicate that γ is closely related to d and h/d. Test results of $\varepsilon_{SE0.5} - \left(\varepsilon_{SE} - \frac{f_{SE}^{'}}{E_c}\right)$ according to d, h/d, and ρ_c are shown in Fig. 7. In Fig. 7 (a), $\varepsilon_{SE0.5} - \left(\varepsilon_{SE} - \frac{f_{SE}^{'}}{E_c}\right)$ linearly decreased with the increase in d, indicating that it decreased by approximately 18% for specimens with h/d of 2, and approximately 31% for specimens with h/d of 1, when d increased by 3 times. $\varepsilon_{SE0.5} - \left(\varepsilon_{SE} - \frac{f_{SE}^{'}}{E_c}\right)$ almost linearly decreased with h/d increased, irrespective of $f_c^{'}$. $\varepsilon_{SE0.5} - \left(\varepsilon_{SE} - \frac{f_{SE}^{'}}{E_c}\right)$ ranged between 0.0026 to 0.0049 for specimens with h/d of 2, and 0.0018 for specimens with h/d of 5.5, indicating that it

Preprints (www.preprints.org) | NOT PEER-REVIEWED | Posted: 22 August 2018 doi:10.20944/preprints201808.0392.v1

252 decreased by 30% to 60% when h/d increased by 2.75 times. In addition, $\varepsilon_{SE0.5}-\left(\varepsilon_{SE}-\frac{f'_{SE}}{E_c}\right)$
253 increased with the increase in ρ_c, and its increasing rate according to f'_c was almost constant.
254 $\varepsilon_{SE0.5}-\left(\varepsilon_{SE}-\frac{f'_{SE}}{E_c}\right)$ ranged between 0.002 to 0.0038 for LWC (ρ_c = less than 2000 kg/m³), and 0.0029
255 to 0.0044 for HWC (ρ_c = more than 2500 kg/m³). These imply that the descending branch behavior
256 in the stress–strain relationship for unconfined concrete is considerably affected by functions of d,
257 h/d, and ρ_c. Based on this analysis, $\varepsilon_{SE0.5}-\left(\varepsilon_{SE}-\frac{f'_{SE}}{E_c}\right)$ was generalized as functions of G_F, f'_{SE},
258 h/d and ρ_c (Fig. 8), using regression analysis from the test results [4, 5, 12–25] for 45 datasets for
259 LWC, 85 datasets, for NWC, and 24 datasets for HWC.

260
$$\varepsilon_{SE0.5}-\left(\varepsilon_{SE}-\frac{f'_{SE}}{E_c}\right)=0.0028\exp\left[1.8\times1000\left(\frac{{G_F}^{0.4}}{{f'_{SE}}^{1.4}\,d^{0.6}}\left(\frac{h}{d}\right)^{-1.2}\left(\frac{\rho_c}{2300}\right)^{2}\right)\right] \quad (18)$$

261 Where the CEB-FIP model [27] for G_F that includes functions of d_a and f'_c, was used as
262 follows.

263
$$G_F=G_{F0}\left(\frac{f'_c}{10}\right)^{0.7} \quad (19)$$

264

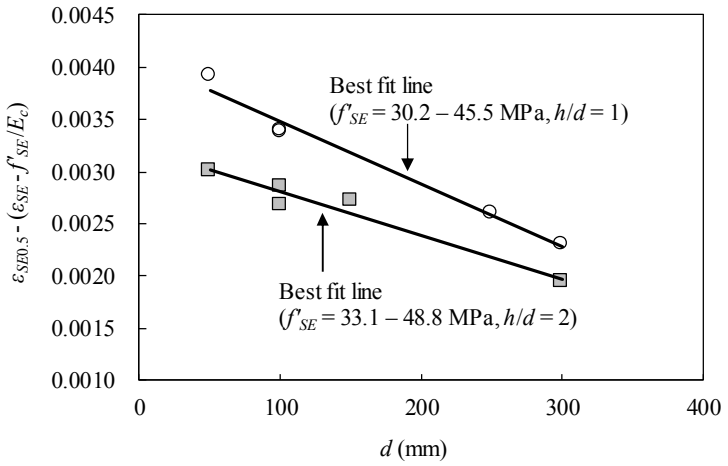

265
266 (a) Width (d)

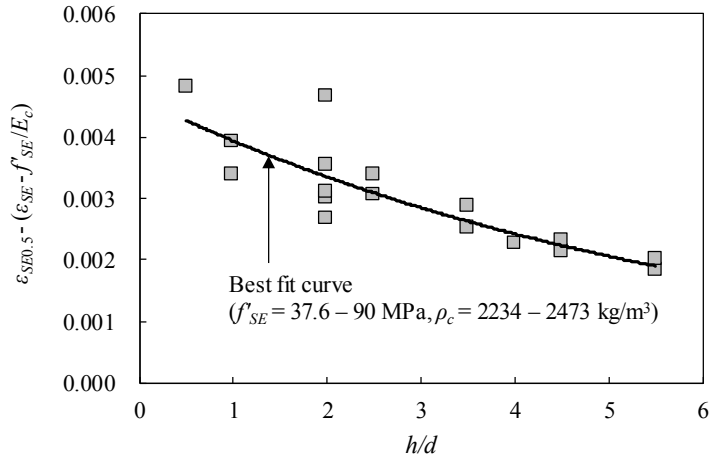

267
268 (b) Aspect ratio (h/d)

Preprints (www.preprints.org) | NOT PEER-REVIEWED | Posted: 22 August 2018 doi:10.20944/preprints201808.0392.v1

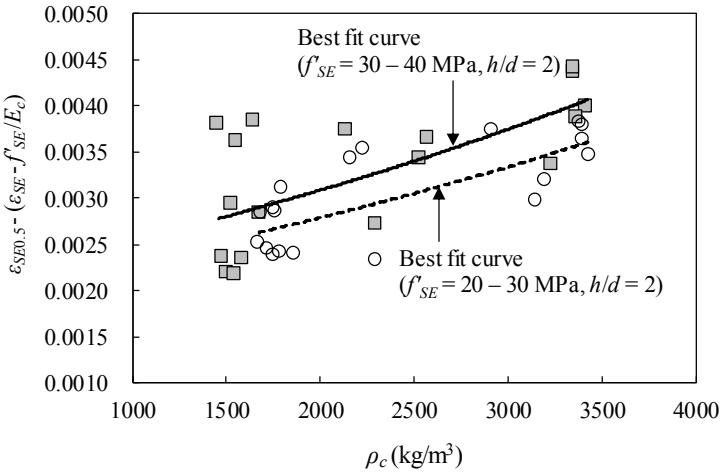

(c) Unit weight (ρ_c)

Figure 7. Variation in $\varepsilon_{SE0.5}$ in softening behavior

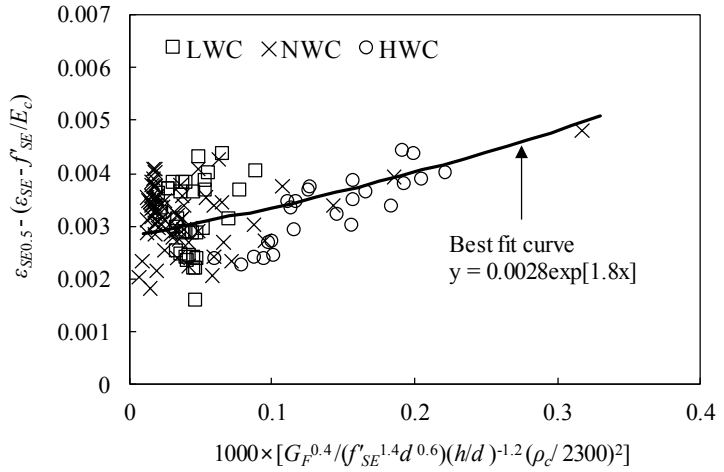

Figure 8. Nonlinear regression analysis to determine $\varepsilon_{SE0.5}$.

where G_{F0} is 0.025 N/mm, 0.03 N/mm and 0.05 N/mm for d_a of 8 mm, 16 mm, and 32 mm, respectively. β_1 in the descending branch can be solved using Eq. (12) and Eq. (18). The solution of β_1 in the descending branch was also calculated using the Newton–Raphson method as in the ascending branch. Finally, the key parameter β_1 was formulated using the analytical parametric study. In the analytical parametric study, $f_c^{'}$, d, h/d, d_a, and ρ_c were selected from 10 MPa to 180 MPa, 50 mm to 500 mm, 0.5 to 5, 4 mm to 25 mm and 1400 kg/m^3 to 4000 kg/m^3, respectively. From the analytical results, statistical optimization was performed to generalize the key parameter β_1 that determines the slope of the descending branch as follows (Fig. 9).

$$\beta_1 = 0.83\left[\left(\frac{f'_{SE}}{10}\right)^{0.62}\left(\frac{d}{150}\right)^{0.2}\left(\frac{h}{d}\right)^{0.35}\left(\frac{2300}{\rho_c}\right)^{1.2}\right]^{1.3} \quad \text{for} \quad \varepsilon_c > \varepsilon_{SE} \tag{20.a}$$

Finally, the stress–strain relationship for unconfined concrete can be proposed as follows.

$$f_c = \left[\frac{(\beta_1+1)\left(\frac{\varepsilon_c}{\varepsilon_{SE}}\right)x}{\left(\frac{\varepsilon_c}{\varepsilon_{SE}}\right)^{\beta_1+1}+\beta_1}\right]f'_{SE} \tag{21}$$

Preprints (www.preprints.org) | NOT PEER-REVIEWED | Posted: 22 August 2018 doi:10.20944/preprints201808.0392.v1

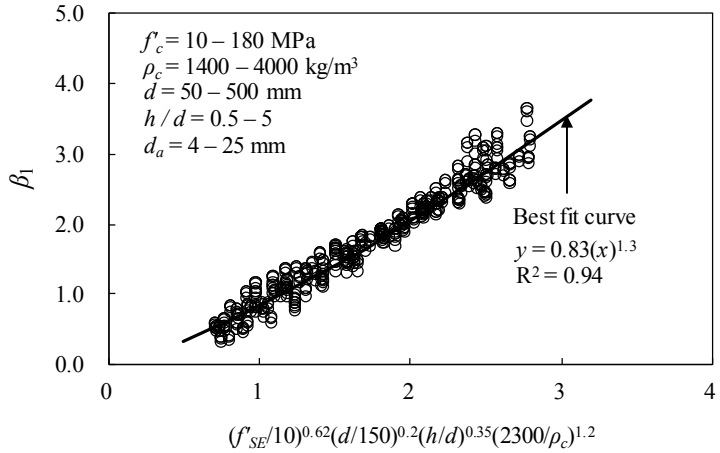

Fig. 9–Formulation of key parameter β_1 in descending branch

where ε_{SE} is given by Eq. (12), f'_{SE} is given by Eq. (5), and key parameter β_1 is given by Eq. (13) or (20). The proposed stress–strain relationship for unconfined concrete can consider the size effect on concrete in the ascending and descending branch, using the power functions of the key parameter β_1 and f'_{SE}.

4. Comparisons with test results

The test results compiled from the available literatures [4, 5, 12–25] were compared with predictions of this study and the existing models [1, 6, 7, 11]. The existing models for the strain–stress relationship proposed by Markeset and Hilleborg [6], and Samani and Attard [7] were selected as summarized in Table 2. Figure 10 shows comparisons of the predicted and measured stress–strain curves [4, 12–18]. The comparative analysis focused on the effect of d, h/d, ρ_c, and f'_c on the stress–strain curve. Table 3 summarizes the normalized root–mean–square error (NRMSE) obtained from the comparisons of test results with predictions. In Table 3, γ_m and γ_s are the mean and standard deviation of the NRMSE, respectively. It is noteworthy that the comparisons of test results with the predictions of Markeset and Hilleborg [6] were conducted only in the descending branch, because Markeset and Hilleborg's model [6] provides the equations only for the descending branch behavior.

Markeset and Hilleborg [6] idealized the CDZ model considering fracture energy, and proposed the descending branch behavior in the stress–strain relationship. In the CDZ model, the total strain is a combination of the strain (ε) in the region where the undamaged zone elastically unloads after the peak stress, the strain (ε_d) in the region propagated by the longitudinal tensile splitting cracks, and the strain (ω/h) by the diagonal tensile band crack. In the model, ε_d is based on the assumption that inelastic deformation in the damaged zone determines the descending branch behavior. To consider inelasticity in the descending branch, ε_d introduces $\left(\frac{f'_c - f_c}{f'_c}\right)^{0.8}$ as expressed in Eq. (9); nevertheless, the descending branch is predicted as a virtually linear curve (Fig. 10 (a)). However, the shapes of the descending branch measured in the existing test results are primarily curved rather than linear. Hence, the accuracy of Markeset and Hilleborg's model [6] according to the concrete type fluctuates with large deviations. The values of γ_m obtained by Markeset and Hilleborg's model [6] are 0.38 for LWC, 0.29 for NWC, and 0.28 for HWC. In particular, Markeset and Hilleborg's model [6] generally underestimates the compressive stress of HWC. This is because this model does not consider the decreasing effect of the slope for HWC in the descending branch because the factor of k to determine ε_d according to concrete type is 3 and 1, only for NWC and LWC, respectively, without considering HWC.

 doi:10.20944/preprints201808.0392.v1

319 **Table 2.** Summary of stress–strain models considering the size effect.

Researcher	Stress–strain relationship of concrete
Markeset and Hillerborg [6]	Ascending branch: –
	Descending branch: $\varepsilon_h = \varepsilon_0 - \left(\frac{f_c'}{E_c}\right) + \varepsilon_d \frac{2.5d}{h} + \frac{\omega}{h}$ for $h > 2d$; $\varepsilon_h = \varepsilon_0 - \left(\frac{f_c'}{E_c}\right) + \varepsilon_d + \frac{\omega}{h}$ for $h \le 2d$; $\varepsilon_d = \frac{2kG_F}{\gamma(1+k)f_c'}\left(\frac{f_c' - f_c}{f_c'}\right)^{0.8}$; $G_F = 0.00097 f_c' + 0.0418$
Samani and Attard [7]	Ascending branch: $f_c = \left[\frac{A\left(\frac{\varepsilon_c}{\varepsilon_0}\right) + B\left(\frac{\varepsilon_c}{\varepsilon_0}\right)^2}{1 + (A-2)\left(\frac{\varepsilon_c}{\varepsilon_0}\right) + (B+1)\left(\frac{\varepsilon_c}{\varepsilon_0}\right)^2}\right] f_c'$; $A = \frac{E_c \varepsilon_0}{f_c'}$; $B = \frac{(A-1)^2}{0.55} - 1$; $E_c = \left(3320\sqrt{f_c'} + 6900\right)(\rho_c / 2300)^{1.5}$
	Descending branch: $f_c = \left[\left(\frac{f_{ic}}{f_c'}\right)^{\left(\frac{\varepsilon_h - \varepsilon_0}{\varepsilon_{ic} - \varepsilon_0}\right)^2}\right] f_c'$; $\varepsilon_{ic} = \left[2.76 - 0.35\ln(f_c')\right]\varepsilon_0$; $f_{ic} = \left[1.41 - 0.17\ln(f_c')\right] f_c'$; $\varepsilon_h = \varepsilon_0 + (\varepsilon_c - \varepsilon_0)\frac{h_0}{h} + \frac{(f_c - f_c')}{E_c}\left[1 - \frac{h_0}{h}\right] + \varepsilon_d\left(\frac{2d - h_0}{h}\right)$ for $h > 2d$; $\varepsilon_h = \varepsilon_0 + (\varepsilon_c - \varepsilon_0)\frac{h_0}{h} + \frac{(f_c - f_c')}{E_c}\left[1 - \frac{h_0}{h}\right] + \varepsilon_d\left(1 - \frac{h_0}{h}\right)$ for $h \le 2d$; $\varepsilon_d = \frac{2kG_F}{\gamma(1+k)f_c'}\left(\frac{f_c' - f_c}{f_c'}\right)^{0.8}$; $G_F = 0.00097 f_c' + 0.0418$
	$\varepsilon_0 = \frac{f_c'}{E_c}\frac{\mu_1}{\sqrt[4]{f_c'}}$; μ_1 = 4.26 for crushed aggregates, and 3.78 for gravel aggregates.
This study	$f_c = \left[\frac{(\beta_1 + 1)\left(\frac{\varepsilon_c}{\varepsilon_{SE}}\right)x}{\left(\frac{\varepsilon_c}{\varepsilon_{SE}}\right)^{\beta_1 + 1} + \beta_1}\right] f_{SE}'$; $f_{SE}' = \left[\frac{0.9\sqrt{\left(\frac{h}{d}\right)^{-0.6}}}{\left[1 + 0.017d\left(\frac{\rho_c}{2300}\right)^{-1}\right]^{0.5}} + 0.63\right] f_c'$; $\varepsilon_{SE} = 0.0016\exp\left[220\left(f_{SE}' / E_c\right)\right]$; $E_c = 8470\left(f_c'\right)^{1/3}(\rho_c / 2300)^{1.17}$
	Ascending branch: $\beta_1 = 0.33\exp\left[0.42\left(f_{SE}' / 10\right)(2300/\rho_c)^{1.5}\right]$
	Descending branch: $\beta_1 = 0.83\left[\left(f_{SE}' / 10\right)^{0.62}(d/150)^{0.2}(h/d)^{0.35}(2300/\rho_c)^{1.2}\right]^{1.3}$

320
321

Preprints (www.preprints.org) | NOT PEER-REVIEWED | Posted: 22 August 2018 doi:10.20944/preprints201808.0392.v1

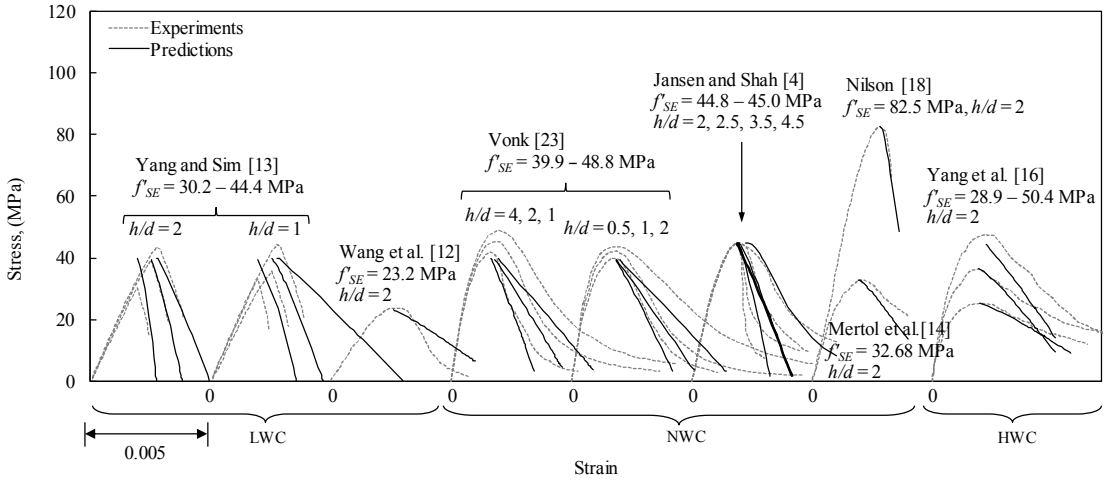

(a) Markeset and Hillerborg [6]

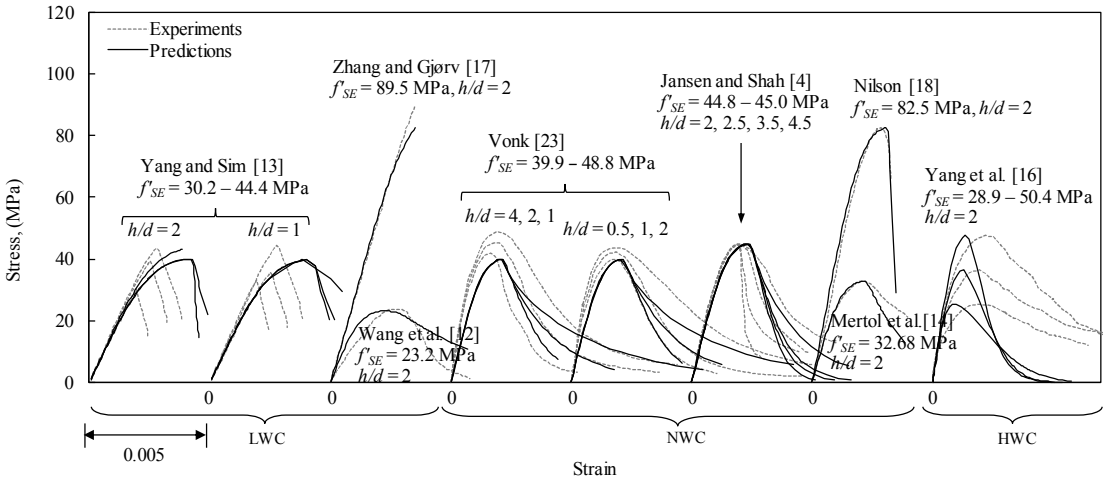

(b) Samani and Attard [7]

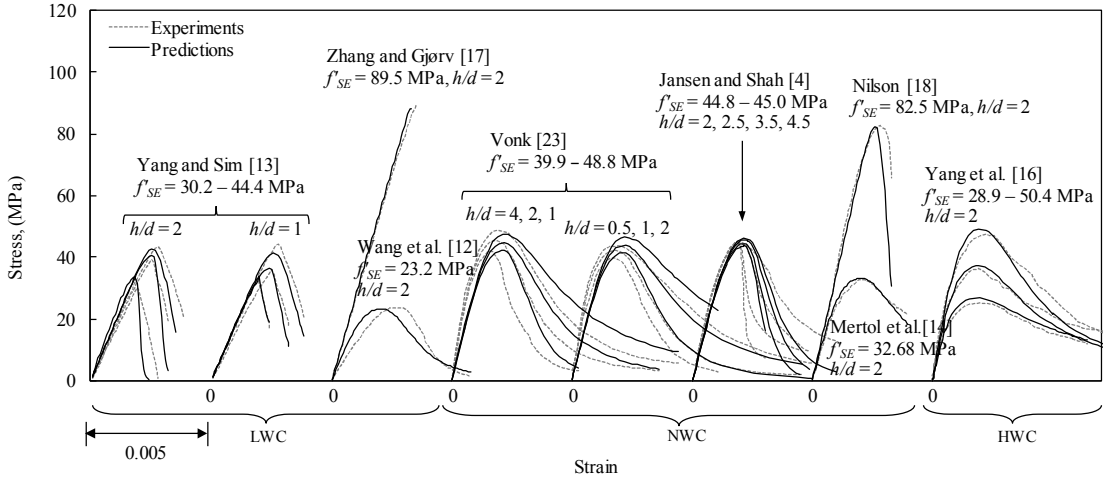

(c) This study

Figure 10. Typical comparisons of predicted and measured stress–strain curves

Table 3. Comparisons of normalized root–mean–square error.

Concrete type	Aspect ratio	Statistical value	Researcher		
			Markeset and Hillerborg [6]	Samani and Attard [7]	This study
LWC	1	γ_m	0.49	0.45	0.21
		γ_s	0.34	0.11	0.10
	2	γ_m	0.28	0.37	0.26
		γ_s	0.24	0.17	0.23
	Subtotal	γ_m	0.38	0.41	0.24
		γ_s	0.13	0.29	0.16
NWC	0.5~1.0	γ_m	0.32	0.23	0.13
		γ_s	0.12	0.07	0.02
	2~2.5	γ_m	0.29	0.20	0.16
		γ_s	0.17	0.16	0.10
	3.5~4	γ_m	0.24	0.33	0.36
		γ_s	0.03	0.03	0.08
	Subtotal	γ_m	0.29	0.22	0.18
		γ_s	0.14	0.14	0.11
HWC	2	γ_m	0.28	0.71	0.10
		γ_s	0.14	0.09	0.01
Total		γ_m	0.31	0.33	0.18
		γ_s	0.19	0.21	0.12

Samani and Attard [7] applied the size effect to the equations for the descending branch proposed by Attard and Setunge's model [11]. As summarized in Table 2, the descending branch behavior proposed by Samani and Attard [7] is also based on the CDZ model and its strain equation is similar to that of Markeset and Hilleborg' s model [6]. In addition, Markeset and Hilleborg's model [6] for ε_d composed of functions of k, γ, and G_F is used without modification. The descending branch behavior in Samani and Attard's model [7], however, is different from that in Markeset and Hilleborg [6], indicating that it is predicted as a curve with an inflection point. As shown in Fig. 10 (b), the ascending branch behavior composed of functions $f_c^{'}$ and ρ_c in Samani and Attard's model [7] is identical to that in Attard and Setunge's model [11]. In the descending branch behavior of Samani and Attard's model [7], the increasing effect of the decreasing slope is explained well with the increase in h/d, as shown in Fig. 10 (b). However, Samani and Attard's model [7] underestimates the compressive stress for HWC. This is because, in this model, the factor k related with the material property does not consider the decreasing effect of the descending slope for HWC. This implies that the factor k in Samani and Attard's model [7] requires calibration using additional test results. In addition, because Samani and Attard's model [7] does not consider the size effect on the peak stress, it overestimates the compressive strength of concrete for LWC. The overestimation increased with the increase in d. The values of γ_m obtained by Samani and Attard's model [7] are 0.41 for LWC, 0.22 for NWC, and 0.71 for HWC.

The proposed model in this study show better agreement with test results, irrespective of d, h/d, concrete type, and $f_c^{'}$. The values of γ_m and γ_s are 0.24 and 0.16 for LWC, 0.18 and 0.11 for NWC, and 0.10 and 0.01 for HWC, respectively. The results are lower than those of the models of

Markeset and Hilleborg [6], and Samani and Attard [7]. The proposed values of γ_m and γ_s are 0.18 and 0.12, respectively, which are the lowest among other models. Based on the CDZ model, a rational stress–strain model for unconfined concrete considering the size effect is proposed, using the key parameter β_1 formulated by functions of f'_{SE}, d, h/d, and ρ_c.

6. Conclusions

From the proposed stress–strain relationship model for various unconfined concrete types considering the size effect based on the CDZ model, the following conclusions were derived.

(1) The existing models do not consider the increasing effect of the descending branch slope with the increase in the aspect ratio and specimen width. In particular, this trend was more notable in LWC than NWC.

(2) The elastic modulus of concrete typically defined in the elastic region where no cracks occurred was not affected by the size effect, whereas the strain at the peak stress affected by the size effect was formulated by an exponential function of f'_{SE}/E_c.

(3) The key parameter β_1 determining the slope of the ascending branch could be proposed as an exponential function of $\left(f'_{SE}/10\right)(2300/\rho_c)^{1.5}$.

(4) In the descending branch, $\varepsilon_{SE0.5}-\left(\varepsilon_{SE}-\frac{f'_{SE}}{E_c}\right)$ could be expressed as an exponential function of $1000\times\left(\frac{G_F{}^{0.4}}{f'_{SE}{}^{1.4}d^{0.6}}\left(\frac{h}{d}\right)^{-1.2}\left(\frac{\rho_c}{2300}\right)^2\right)$, considering the influencing parameters of specimen width, aspect ratio, and concrete density.

(5) The key parameter β_1 determining the slope of the descending branch reasonably considered the size effect by formulating as an exponential function of $\left(\frac{f'_{SE}}{10}\right)^{0.62}\left(\frac{d}{150}\right)^{0.2}\left(\frac{h}{d}\right)^{0.35}\left(\frac{2300}{\rho_c}\right)^{1.2}$, based on the CDZ model.

(6) The proposed model of the stress–strain relationship for unconfined concrete showed good agreements with the test results, irrespective of specimen width, aspect ratio, concrete density, and compressive strength.

Author Contributions: JH.M. and Y.L. conducted the analysis of datasets compiled in this study. KH.Y. designed project. All authors contributed to the comprehensive analysis and conclusion.

Funding: This research funded by Ministry of Land, Infrastructure and Transport of the Korean government.

Acknowledgments: This research was supported by the Research Grant from (Kyonggi University) through the Korea Agency for Infrastructure Technology Advancement funded by the Ministry of Land, Infrastructure and Transport of the Korean government(Project No.: 18TBIP-C126470-02).

Conflicts of Interest: The author declares that there is no conflict of interests regarding the publication of this paper.

References

1. Yang, K.H.; Mun, J.H.; Cho, M.S.; Kang, T.H–K. Stress–strain model for various unconfined concretes in compression. *ACI Struct. J.* 2014, 111, 819–826.
2. Almusallam, T.H.; Alsayed, S.H. Stress–strain relationship of normal, high-strength and lightweight concrete. *Mag. Concr. Res.* 1995, 47, 39–44.
3. Lu, Z.H.; Zhao, Y.G. Empirical stress–strain model for unconfined high-strength concrete under uniaxial compression. *J. Mater. Civ. Eng. ASCE.* 2010, 22, 1181–1186.
4. Jansen, D.C.; Shah, S.P. Effect of length on compressive strain softening of concrete. *J. Eng. Mech.* 1997, 123, 25–35.
5. Sim, J.I.; Yang, K.H.; Kim, H.Y.; Choi, B.J. Size and shape effects on compressive strength of lightweight concrete. *Constr. Build. Mater.* 2013, 38, 854–864.

6. Markeset, G.; Hillerborg, A. Softening of concrete in compression–localization and size effects. *Cem. Concr. Res*. 1995, 25, 702–708.
7. Samani, A.K.; Attard, M.M. A stress–strain model for uniaxial and confined concrete under compression, *Eng. Struct*. 2012, 41, 335–349.
8. Bazant, Z.P.; Planas, J. *Fracture and size effect in concrete and other quasibrittle materials*; CRC Press: New York, 1998.
9. Bazant, Z.P. Size effect in blunt fracture: concrete, rock, metal. *J. Eng. Mech. ASCE*. 1984, 110, 518–535.
10. Kim, J.K.; Eo, S.H. Size effect in concrete specimens with dissimilar initial cracks. *Mag. Concr. Res*. 1990, 42, 233–238.
11. Attard, M.; Setunge, S. Stress–strain relationship of confined and unconfined concrete. *ACI Mater. J*. 1996, 93, 432–442.
12. Wang, P.T.; Shah, S.P.; Naaman, A.E. Stress–strain curves of normal and lightweight concrete in compression. *ACI J*. 1978, 75, 603–611.
13. Yang, K.H.; Sim, J.I. Modeling of the mechanical properties of structural lightweight concrete based on size effects. Technical Report, Department of Plant·Architectural Engineering, Kyonggi University, Suwon, South Korea, 2011. (in Korean)
14. Mertol, H.C.; Kim, S.J.; Mirmiran, A.; Rizkalla, S.; Zia, P. Behavior and design of HSC members subjected to axial compression and flexure. Proceedings of the 7th International Symposium on Utilization of High-Strength/High–Performance Concrete, SP-228, H.G. Russell ed., American Concrete Institute, Farmington Hills, MI, 2005; pp. 395–420.
15. Zhang, M.H.; Gjørv, O.E. Mechanical properties of high strength lightweight concrete. *ACI Mater. J*. 1991, 88, 240–247.
16. Yang, K.H.; Mun, J.S.; Lee, H. Workability and mechanical properties of heavyweight magnetite concrete. *ACI Mater. J*. 2014, 111, 273–282.
17. Wee, T.H.; Chin, M.S.; Mansur, M.A. Stress–strain relationship of high-strength concrete in compression. *J. Mater. Civ. Eng. ASCE*. 1996, 8, 70–76.
18. Nilson, A.H. High–strength concrete: an overview of Cornell research, Proceedings of Symposium on Utilization of High–Strength Concrete, Stavanger, Norway, 1987; pp. 27–37.
19. Yi, S.T.; Kim, J.K.; Oh, T.K. Effect of strength and age on the stress–strain curves of concrete specimens. *Cem. Concr. Res*. 2003, 33, 1235–1244.
20. Liu, T.C. Stress–strain response and fracture of concrete in biaxial compression, Cornell University, 1971.
21. Tomaszewicz, A.; Betongens, A.SINTEF Report No STF 65A84065, Trondheim, 1984.
22. Mun, J.H.; Mun, J.S.; Yang, K.H. Stress–strain relationship of heavyweight concrete using magnetite aggregate. *J. Archit. Inst. Korea*, 2013, 29, 85–92. (in Korean)
23. Vonk, R. Softening of concrete loaded in compression. Ph.D. thesis, Eindhoven University of Technology, The Netherlands, 1992.
24. Lee, K.H.; Yang, K.H.; Mun, J.H.; Kwon, S.J. Mechanical properties of concrete made from different expanded lightweight aggregates. *ACI Mater. J*. 2018, Accepted.
25. Mun, J.S.; Mun, J.H.; Yang, K.H.; Lee, H., Effect of substituting normal-weight coarse aggregate n the workability and mechanical properties of heavyweight magnetite concrete. *J. Korea Concr. Inst*. 2013, 25, 439–446. (in Korean)
26. Taylor, M.A.; Broms, B.B. Shear bond strength between coarse aggregate and cement paste or mortar. ACI Proceedings, 1964, 61, 939–958.
27. Comité Euro-International du Beton (CEB-FIP). *Structural concrete: textbook on behaviour, design and performance*; International Federation for Structural Concrete (fib): Switzerland, 1999.